In situ analysis of phase constituents evolution upon hydrogen cycling of cold-forged Mg-Ni powders

Jing Wen, Laetitia Laversenne, Marc Novelli, Thierry Grosdidier, Patricia de Rango

In situ analysis of phase constituents evolution upon hydrogen cycling of cold-forged Mg-Ni powders

Jing Wen[a,b,c,d], Laetitia Laversenne[a], Marc Novelli[b,c], Thierry Grosdidier[b,c,*], Patricia deRango[a,*]

[a]Université Grenoble Alpes, CNRS, Grenoble INP, Institut Néel, 38000 Grenoble, France

[b]Laboratoire d'Excellence DAMAS, Université de Lorraine, CNRS, 57000 Metz, France

[c]Laboratoire d'Etude des Microstructures et de Mécanique des Matériaux (LEM3), Université de Lorraine, CNRS, Arts et Métiers ParisTech, 57000 Metz, France

[d]School of Materials Science and Engineering, Dalian Jiaotong University, Dalian 116028, China

Abstract

Development of hydrogen storage in metal hydrides requests efficient, simple and safe processes such as room temperature forging. Samples elaborated in this way from Mg and Ni powders result in bulk pellets whose only identified phases are Mg and Ni. Deuterium absorption occurs from 250°C in these samples due to the co-existence of basal fiber texture and structural defects, both induced by forging. In situ neutrons diffraction analysis shows the progressive formation of the $Mg_2NiD_{0.3}$ / Mg_2NiD_4 phases upon deuterium cycling and allows to identify the multi-step absorption and desorption mechanisms at temperatures as low as 270°C. The growth of the $Mg_2NiD_{0.3}$ / Mg_2NiD_4 phases occurs in a short time during the second step of the deuterium absorption – as $Mg_2NiD_{0.3}$ transformed into Mg_2NiD_4 – and progresses from the periphery of the initial Ni particles towards their center. The mechanism is controlled simultaneously by deuterium diffusion and migration of Mg atoms through the already formed Mg_2NiD_4 deuteride. The reaction between Mg and Ni is not observed in the absence of deuterium, even after annealing at 285°C for 48 hours, thus we evidence a deuterium-induced mobility of the metal atoms.

Keywords: Hydrogen absorbing materials; Magnesium; Nickel; Forging; Kinetics; Neutron diffraction.

Corresponding authors: Patricia de Rango, patricia.derango@neel.cnrs.fr

1. Introduction

Magnesium and its alloys have attracted significant interest in the field of hydrogen storage owing to their high hydrogen-storage capacity, low-cost and abundance in Earth's crust. However, the high thermodynamic stability of Mg-H bond as well as sluggish sorption kinetics limit their practical applications [1-3]. Many efforts have been devoted to modify the sorption properties of Mg-based materials [4]. High Energy Ball Milling (HEBM) of MgH_2 powders with the addition of 3d-transition metal or oxides – which play the role of catalysts in the sorption reactions – is widely used [5-8]. Among the commonly used 3d transition metals, nickel (Ni) acts as an efficient promoter of hydrogen sorption kinetics [8]. Mechanical alloying was also successfully applied starting from a mixture of Mg and Mg_2Ni powders to improve the hydrogenation/dehydrogenation rate of Mg/MgH_2. It is established that the presence of the Mg_2Ni phase can play a catalytic role on the formation of MgH_2 [9]. Moreover, a remarkable synergetic effect has been evidenced in a composite material in which the desorption temperature of MgH_2 can be lowered by about 100 K thanks to the presence of Mg_2NiH_4 [10]. This effect certainly results from the lower thermodynamic stability of Mg_2NiH_4 as compare to MgH_2. Nevertheless, when large-scale production is desired, the HEBM processes are prohibitive as they are time- and energy-consuming, and require substantial manpower. In addition, the handling of these pyrophoric powders poses serious safety problems.

Several processes such as melt-spinning [11,12] and Severe Plastic Deformation (SPD) [13] were then carried out to improve the hydrogenation/dehydrogenation rates in Mg-based materials in order to induce microstructure refinement, texture and/or specific grain boundaries in "bulk" nano-materials, while avoiding the problem associated with surface reactivity [14-15]. Among these studies, SPD processes have been widely applied to Mg-Ni alloys, including Equal Chanel Angular Pressing (ECAP) [16-18], High Pressure Torsion (HPT) [19-24] and Cold Rolling [25, 26].

Forging, the ancestral metalwork technique, was also carried out at room temperature starting from MgH_2 powders [27,28]. In a previous study [29], the authors have investigated how forging can induce high sorption performance while offering a safe and efficient route to manufacture Mg-based materials at large-scale. The samples were prepared from a precursor made of compacted powders of Mg and Ni mixed in proportions close to those of the Mg-rich eutectic (T_m = 506°C). More recently, different forging conditions were used to consolidate Mg + Ni powders in order to improve the hydrogen storage properties through microstructure optimization [30]. A strong impact of the applied forging conditions was observed. Samples forged at elevated temperature, close to the melting point, displayed the fastest desorption - which was ascribed to the formation of Mg_2Ni upon forging - but their absorption kinetics remained rather slow. In contrast, powder samples cold forged at room temperature exhibited rather fast absorption kinetics promoted by a strong fiber texture [30] and internal strains induced in the brittle state of Mg, but slow desorption kinetics because no Mg_2Ni had formed at room temperature. Eventually, samples submitted to a previous annealing followed by cold forging exhibited the best compromise for absorption, including a fast activation (first absorption), as well as an improved desorption. The sorption properties of these annealed and forged samples were the subject of an in-depth study performed *in situ* by neutron diffraction that will be discussed elsewhere [31]. Nevertheless, the direct forging of compacted powders at room temperature offers a clear advantage in large-scale production, because it allows to avoid a previous annealing under protective atmosphere. Moreover, while samples forged directly at room temperature contain only the Mg and Ni phases after forging, we have shown that Ni reacts with magnesium during hydrogen cycling at 310°C to form a Mg_2Ni related phase, leading to a progressive improvement of the sorption kinetics [29]. This recombination was not expected at such a low temperature, where metal atoms mobility is very slow.

The purpose of the present contribution is to analyze results of *in situ* neutron diffraction experiments performed under deuterium atmosphere from a Mg + Ni composite consolidated by cold forging in order to identify which sorption conditions are beneficial to the growth of the Mg_2Ni and/or Mg_2NiH_4 phases at such a relatively low temperature. Electron microscopy of the partially deuterated sample was also used to elucidate the formation mechanisms of these phases at a microstructural scale.

2. Experimental

2.1 Sample preparation

Atomized Mg powder having a 30 - 40 µm spherical particle shape, produced by the SFM Company, Switzerland (99.8 wt % purity) and nickel powder of about 5 - 10 µm produced by Neyco, France (99.5 wt % purity) were used as starting materials. Prior to forging at room temperature, samples were prepared using the following procedures. Firstly, batches of Mg-22 wt % Ni powders were mixed by manual grinding in a glove box under argon atmosphere. Subsequently, this mixture was compacted in a die applying a pressure of about 100 MPa. These compacted powders in the form of pellets are referred to as starting materials in the present work. Finally, forging was done on 3 pellets (13 mm in diameter) that were inserted into a thin cylindrical stainless-steel sheath (22 mm height and 0.5 mm wall thickness) to avoid a burst effect at shock [29]. The cold forging was carried out at room temperature in an open die, using a 150 kg hammer dropped from a height of 1.5 m at a rate of 4.7 m/s with a device initially designed for hard magnets elaboration [32]. A single pass was applied, and the height of the specimen was reduced from 22 to 5.5 mm, which corresponds to a reduction rate of 75%.

2.2 Deuterium sorption and phases characterization

For *in situ* neutron diffraction, the sample (2.00 g) was broken into small parts and poured into the 8 mm diameter molybdenum sample holder. The Mo airtight sample holder was equipped

with a valve and a stainless-steel capillary tube that was connected to a Sievert apparatus from Hiden-Isochema allowing sorption measurements in the course of the neutron diffraction experiment. Deuterium (D_2) was used in place of hydrogen to dispense from its high incoherent scattering. The sample temperature was monitored by the use of an external thermocouple placed above the sample-holder, the all being inserted into a vanadium furnace. Neutron powder diffraction was performed at the CRG-D1b diffractometer at the Institute Laue Langevin (ILL) neutron source in Grenoble (France) with λ = 2.52 Å. *In situ* diffraction patterns were recorded during the heating step under dynamic vacuum up to a set point of 250°C and during several successive deuterium absorption-desorption sequences. The description of deuterium charging-discharging procedures is given in Table 1. Because the amount of deuterium absorbed by the sample was high comparatively to the internal volume of the Sievert apparatus, the internal pressure recorded on desorption increased progressively close to the equilibrium pressure before the full desorption of the sample. It was then necessary to manually reduce the deuterium pressure 2 or 3 times upon desorption, so that the pressure evolved from 0.15 bars to about 1.5 bars. Diffraction patterns were collected every 2 min and analyzed according to the Rietveld method using the FullProf Suite [33].

Table 1 Description of deuterium charging-discharging procedures.

	Charging/Absorption	**Discharging/Desorption**
1st cycle	T= 250 °C, $P(D_2)$ = 20 bars, lasting for 400 minutes	T = 270 °C, 0.15 < $P(D_2)$ < 1.5 bar lasting for 90 minutes
2nd cycle	T= 270 °C, $P(D_2)$ = 20 bars, lasting for 270 minutes	T = 270 °C, 0.5 < $P(D_2)$ < 1.5 bar, $P(D_2)$ decreased at 55 min. and at 115 min. T increased to 285°C at 115 min. lasting for 180 min Dynamic vacuum lasting for 240 min.

3rd cycle	T= 285 °C, $P(D_2)$ = 20 bars, lasting for 120 minutes	T = 285 °C, 0.15 < $P(D_2)$ < 1.5 bar $P(D_2)$ decreased at 40 min. lasting for 100 minutes
4th abs.	T= 285 °C, $P(D_2)$ = 20 bars, lasting for 60 minutes	

The phase composition and microstructure investigations before and after deuterium charging were carried out by using a combination of X-Ray Diffraction (XRD) analysis and scanning electron microscopy (SEM) observations coupled with electron backscatter diffraction (EBSD) mapping. The samples were mechanical polished using SiC papers with grits from 1000 to 4000 followed by electrolytic polishing in an electrolyte of 62% phosphoric acid and 38% ethanol at 2 V for 3 min, at −15 °C. To collect high-quality Kikuchi patterns, the samples were Ar ion polished with a PECS-II GATAN using 3.0 keV beam energy under dual beam condition, with gun angle of 2° and for about 2 h. Then EBSD characterization was performed at a step size of 100 nm using a field emission JEOL-6500F SEM equipped with the AZtec acquisition software package.

3. Results

3.1 Phase and texture analysis before deuterium charging

The XRD patterns recorded on the surface of the compacted powders and after forging on a surface perpendicular to the forging direction are shown in Fig. 1a. Only the initial phases Mg and Ni and a very low amount of MgO were detected before and after forging, indicating that no phase transformation occurs under the impact loading at room temperature. It is interesting to notice however that the relative intensity of the Mg peaks was modified with the (0002) peak becoming more intense after the cold deformation. As already reported in [30], where the texture analysis was presented, since plastic deformation is dominated by magnesium for the

powder mixture, the forged sample is characterized by a majority of Mg grains having <0001> direction approximately parallel to the forging direction (Fig. 1b). The formation of this {0001} basal fiber texture is related to the slip systems $\{0001\}\langle 11\bar{2}0 \rangle$ operating on the basal planes [34].

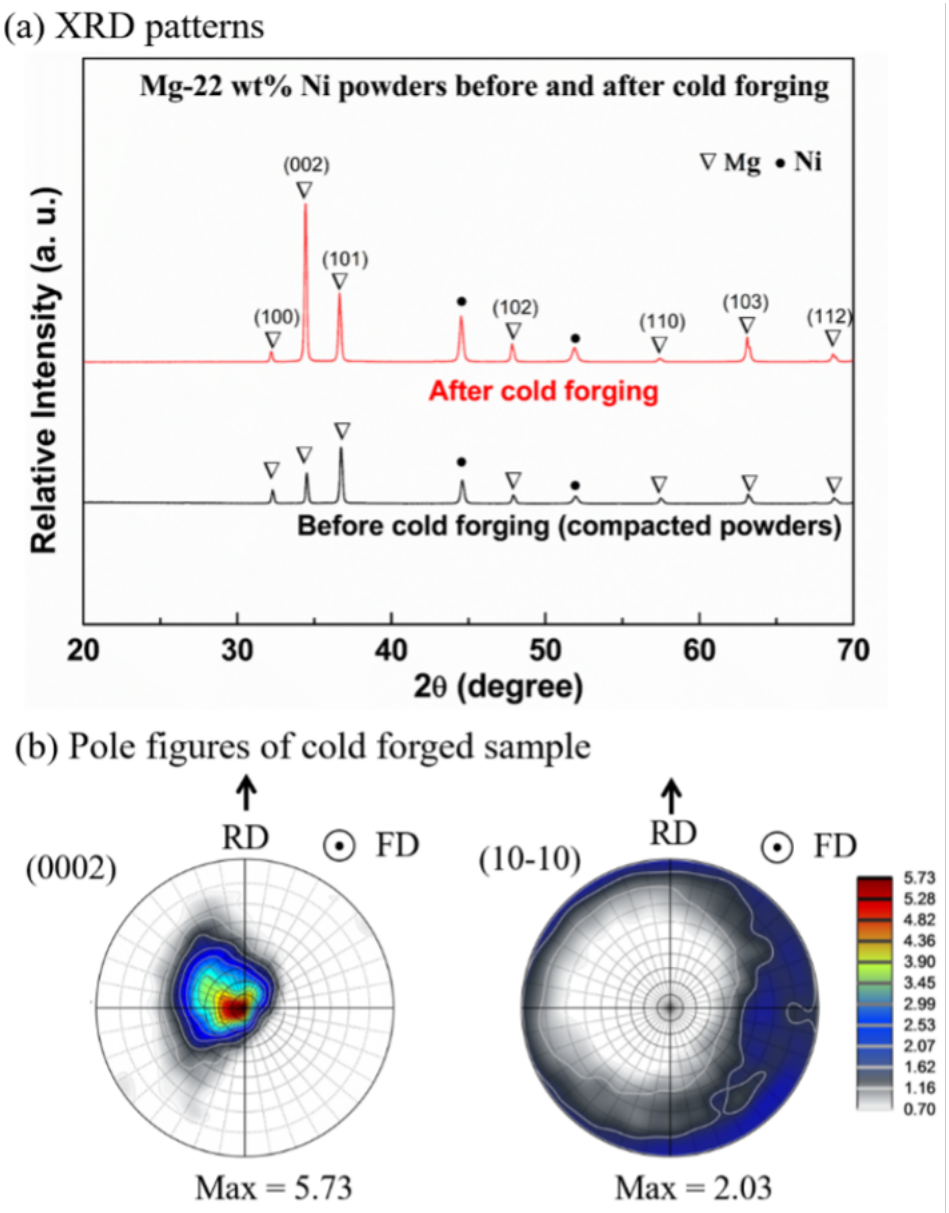

Fig. 1: XRD patterns of Mg-22wt% Ni powder before and after cold forging (a) and pole figure of Mg-phase after cold forging meaured by XRD (b) [17].

3.2 Deuterium sorption kinetics and phases evolution investigated by in situ neutron diffraction

3.2.1 Deuterium absorption

Fig. 2 shows the kinetics curves of deuterium uptake (Fig. 2a) and the *in-situ* neutron diffraction patterns recorded after 60 min of charging (Fig. 2b) during each absorption process. As describe in Table 1, absorptions were performed under a pressure of 20 bars, and deuterium was released from the sample prior to each loading.

Forging the Mg-Ni powder sample at room temperature allows the first deuterium absorption (Abs1) to occur at a temperature as low as 250°C, which is 100°C lower than for the "standard" micrometric Mg powders [35, 36]. Since the deuterium uptake kinetics was rather slow at $T = 250$°C, only approximately 4.0 wt % of deuterium was absorbed after 300 minutes of deuterium charging. It should be mentioned that due to a technical problem, it was not possible to record the hydrogen up-take at the beginning of this first stage of absorption. As the charging temperatures for the second absorption (Abs2) and third absorption (Abs3) were increased to $T = 270$°C and $T = 285$°C respectively, the deuterium uptake kinetics were largely improved.

The *in situ* neutron diffraction patterns collected after 60 min of deuterium charging for each cycle (Fig. 2b), shows two peaks positioned at $2\theta = 70°$ and 105° which arise from the molybdenum sample holder. The diffraction pattern recorded at 250°C under vacuum (i.e., without charging) is also given for comparison. After heating under vacuum for 60 min, only the initial phases Mg and Ni were detected, indicating that no Mg_2Ni phase was formed because the temperature of 250°C was insufficient to promote interdiffusion of Mg and Ni. Submitting the sample to a pressure of 20 bars at 250°C (Abs1) induces magnesium deuteration, as can be seen from the additional peaks corresponding to MgD_2 in the neutron diffraction pattern. As the charging temperature for Abs2 and Abs3 increased to $T = 270$ °C and $T = 285$ °C, the diffraction peaks corresponding to Mg_2NiD_4 phase became clearly visible, whereas they were not

detectable after 60 minutes at 250°C. With the increase of temperature, the relative intensities of the diffraction peaks corresponding to the MgD_2 and Mg_2NiD_4 phases became more intense in comparison with the Mg ones.

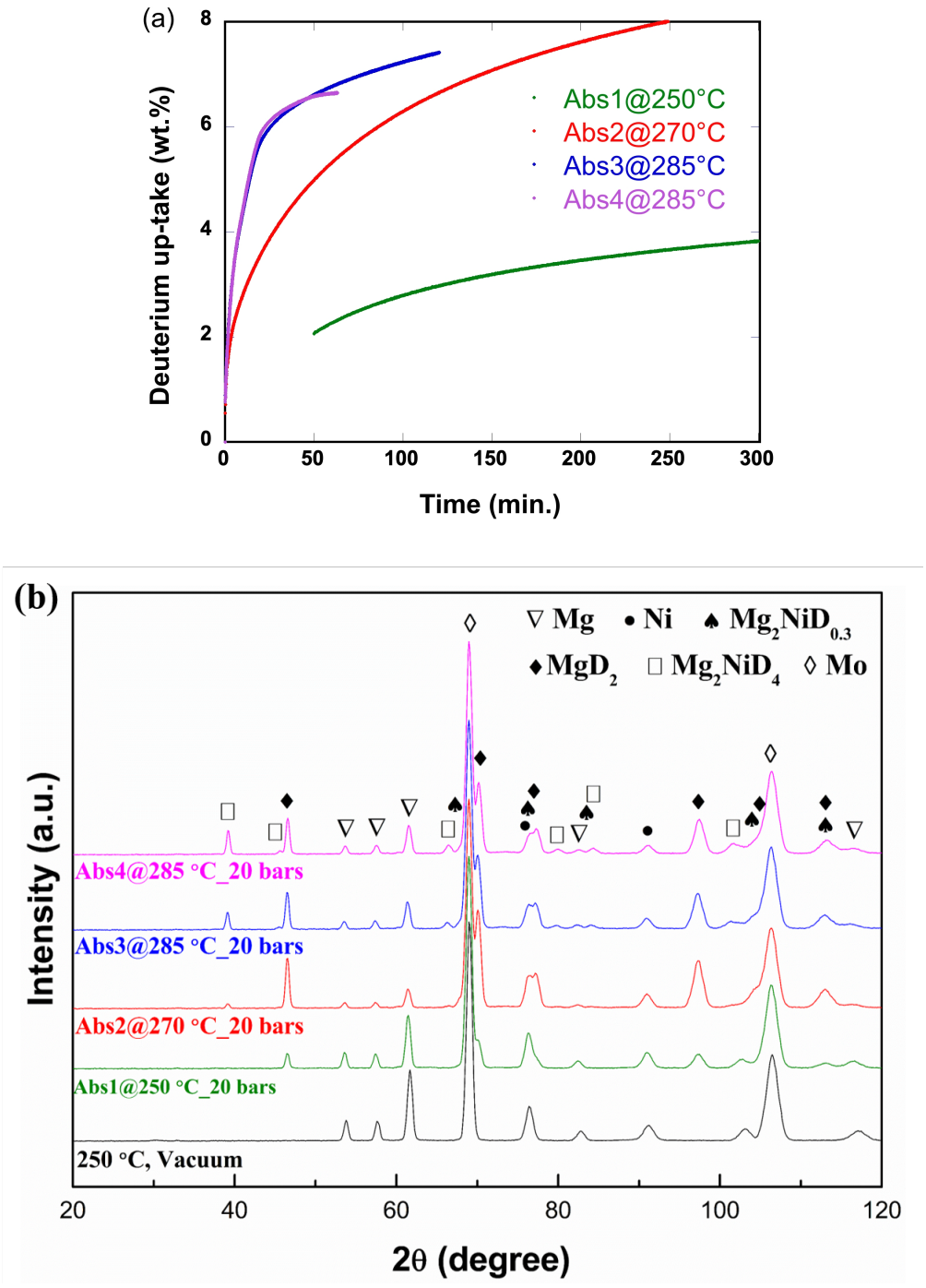

Fig. 2: Kinetic curves of deuterium uptake recorded during each absorption (a) and neutron diffraction patterns collected after 60 min of deuteration for each cycle (b).

The structural analyses were performed using Rietveld refinement of the neutron diffraction patterns. Fig. 3 shows the refined patterns collected at the end of each absorption. The colorful dots and black lines correspond to the measured and calculated profiles respectively, and the blue lines are their corresponding difference. The very limited difference between the observed and the calculated patterns allowed to gain reliable data for each phase constituent. The binary MgD_2 deuteride has a tetragonal body centered (*P42/mnm*) crystal structure. Its lattice parameters were determined to be a = 4.5091 Å and c = 3.0193 Å. The Mg_2NiD_4 phase has a face-centered cubic structure (*Fm-3m*) with lattice parameter of a = 6.5128 Å. Table 2 gives the weight fractions of phase constituent calculated from the Rietveld. These data confirmed that only a very limited amount of Mg_2NiD_4 was formed during the absorption at 250°C, while increasing amounts of Mg_2NiD_4 were detected as the temperature and the sorption cycle increased.

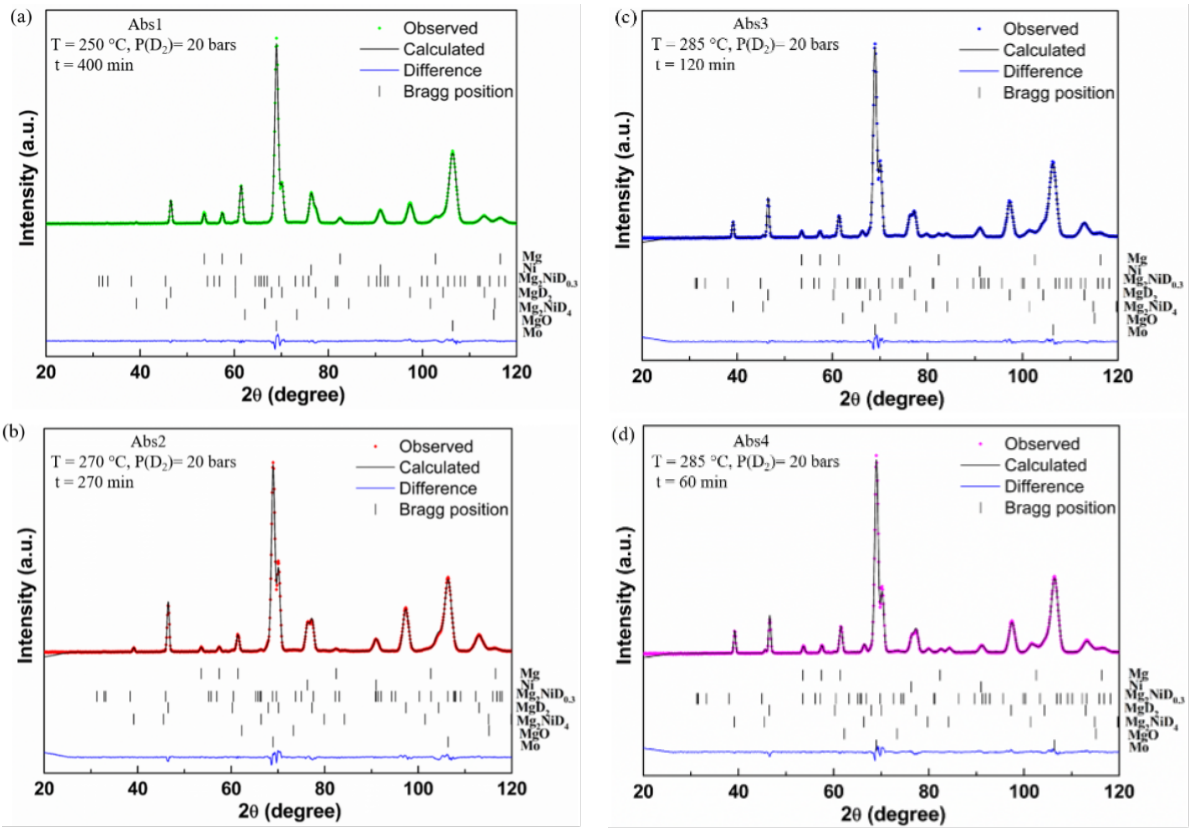

Fig. 3: Rietveld refinements of the neutron diffraction patterns collected at the end of Abs1 (a) and Abs2 (b), Abs3 (c) and Abs4 (d), respectively.

Table 2 Weight fractions of phase constituents calculated from Rietveld refinements of neutron diffraction patterns during deuterium absorption.

	Mg, wt %	Ni, wt %	$Mg_2NiD_{0.3}$, wt %	MgD_2, wt %	Mg_2NiD_4, wt %
Abs1@250 °C					
t = 0 min	74.29 ± 0.56	25.02 ± 0.24	0	0.65 ± 0.07	0
t = 60 min	60.63 ± 0.48	25.30 ± 0.23	0	14.00 ± 0.13	0.03 ± 0.001
t = 120 min	56.56 ± 0.46	25.22 ± 0.22	0	18.05 ± 0.15	0.07 ± 0.01
t = 400 min	49.73 ± 0.42	24.66 ± 0.22	0.06 ± 0.02	24.97 ± 0.17	0.56 ± 0.002
Abs2@270°C					
t = 0	73.74 ± 1.13	22.97 ± 0.28	0.50 ± 0.18	1.05 ± 0.06	0.16 ± 0.07
t = 60 min	40.85 ± 0.95	21.34 ± 0.27	0.57 ± 0.23	33.23 ± 0.35	2.21 ± 0.11
t = 120 min	31.83 ± 0.92	21.28 ± 0.28	0.57 ± 0.25	42.01 ± 0.43	2.48 ± 0.12
t = 270 min	22.64 ± 0.95	20.86 ± 0.30	0.63 ± 0.27	51.13 ± 0.55	2.87 ± 0.14
Abs3@285°C					
t =0 min	71.69 ± 1.25	17.67 ± 0.27	5.64 ± 0.61	2.48 ± 0.08	0.27 ± 0.08
t = 60 min	34.31 ± 1.08	15.00 ± 0.25	0.37 ± 0.33	37.19 ± 0.45	10.61 ± 0.23
t = 120 min	29.36 ± 1.08	14.90 ± 0.27	0.44 ± 0.40	42.08 ± 0.53	10.83 ± 0.25
Abs4@285°C					
t = 0 min	69.72 ± 2.23	12.88 ± 0.42	11.25 ± 0.59	0.85 ± 0.15	0 ± 0.16
t = 60 min	39.62 ± 0.92	11.96 ± 0.23	1.30 ± 0.30	35.66 ± 0.41	15.21± 0.23

In order to correlate the phase constituent dependence with absorption kinetics, the deuterium uptake curve and the changes in phase content are superimposed on the same plot in Fig. 4. Note that, because the kinetics of phase transformations increased with temperature and numbers of cycles, the time scales of the different figures are different. For the first deuterium absorption at T = 250°C (Fig. 4a), only one-third of Mg transformed into MgD_2 after 400 min of deuterium charging, due to the sluggish diffusion activity of deuterium atoms at low temperature. As the charging temperature for the second absorption increased to T = 270°C (Fig. 4b), and because the sample was partially activated after the first sorption cycle, the formation of MgD_2 was largely accelerated. As indicated in Fig. 4b, two-third of Mg transformed into MgD_2 within 270 minutes of deuterium charging. The sample took up about 8.01 wt % of deuterium upon this second absorption, which is twice the amount of deuterium achieved during the first absorption. During the second absorption, the formation of a low amount of Mg_2NiD_4

(about 2.87 wt %) is also observed. This formation is accompanied by a reduction in the proportion of Ni and takes place mainly during the first 10 minutes of the deuterium absorption.

Increasing the deuterium charging temperature to 285°C for the third absorption led to a further acceleration of the absorption kinetics (Fig. 4c). As observed, a three-stage deuterium uptake took place. A change in slope is observed after 10 min while the kinetics became much slower after about 17 minutes. The first rapid stage of absorption is directly related to the formation of the MgD_2 phase in the presence of the $Mg_2NiD_{0.3}$ solid solution resulting from the desorption, since no formation of Mg_2NiD_4 was observed at this stage. The formation of additional MgD_2 phase became more sluggish after about 10 minutes, a time at which the deuterium uptake was also completed via the $Mg_2NiD_{0.3} \rightarrow Mg_2NiD_4$ transformation (stage II). This is visible in the 2D plot representing the neutron diffraction scans in Fig. 4e. For a clearer visualization, only a part of the collected diffraction data is shown with 2θ value ranging from 30 to 65°. It is interesting to notice that the $Mg_2NiD_{0.3} \rightarrow Mg_2NiD_4$ transformation, which occurred between 10 and 17 minutes, was accompanied by an additional formation of Mg_2NiD_4 and a slight decrease in the Ni content within the sample. After 17 min, once the formation of Mg_2NiD_4 was completed, the amount of Ni remained rather constant on charging. After these 17 min of charging, the deuterium uptake was only associated with the formation of additional MgD_2 with a slow kinetics (stage III). The comparison of Fig. 4c and Fig. 4d reveals that the three-stage deuterium uptake behavior - associated with (i) the rapid formation of MgD_2 followed by (ii) both MgD_2 and Mg_2NiD_4 formation and then (iii) the completion of the absorption by MgD_2 solely - was even more obvious during the fourth deuterium absorption as the amount of $Mg_2NiD_{0.3}$ initially present at the beginning of the absorption had increased. Also, it is clear from the data gathered in Table 2 that an additional amount of Mg_2NiD_4 was formed after each absorption while the amount of Ni gradually decreased.

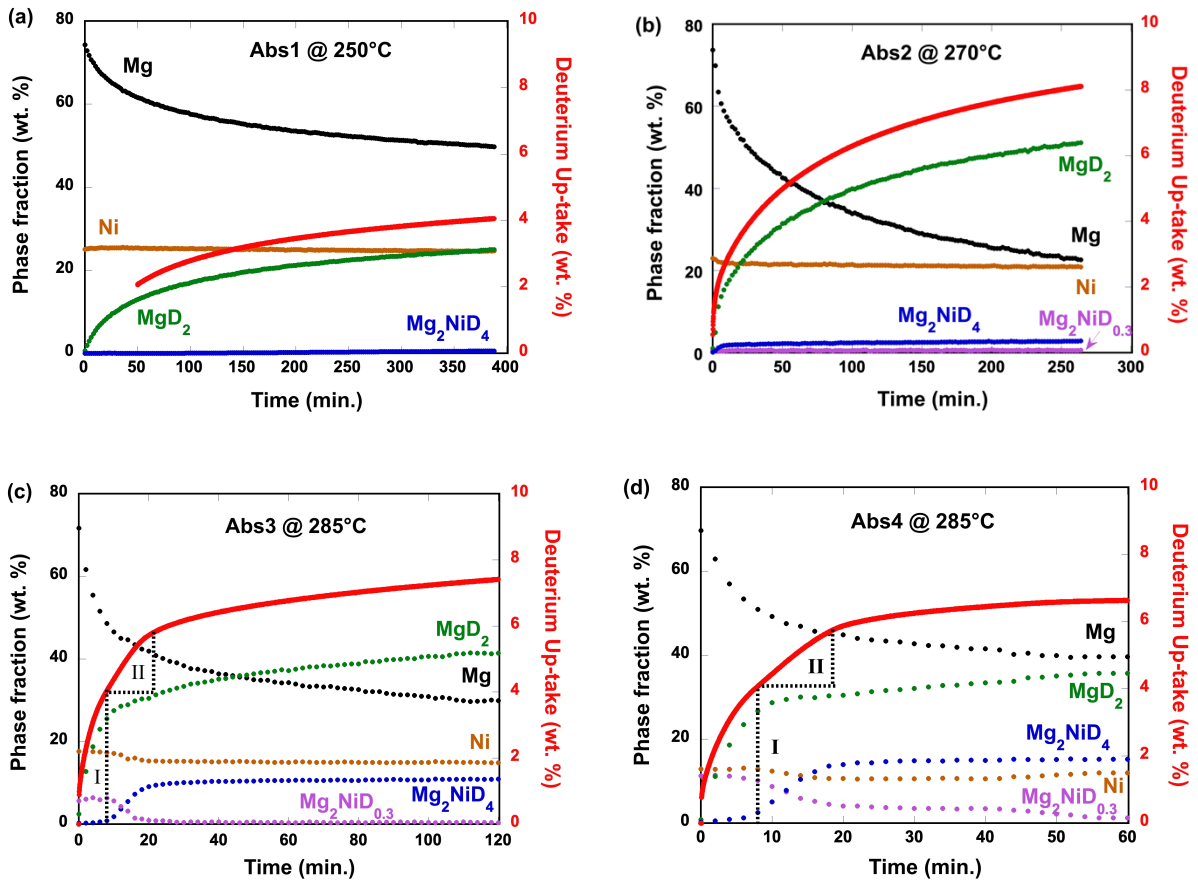

Fig. 4: Deuterium absorption kinetics coupled with phase evolution during each deuterium charging under a deuterium pressure of 20 bars: (a) Abs1 at T = 250 °C, (b) Abs2 at T = 270 °C, (c) Abs3 at T = 285 °C, and (d) Abs4 at T = 285 °C; (e) and (f) correspond to the 2D plots of neutron diffraction patterns recorded during Abs3 and Abs4, respectively. For a clear visualization we show only a part of the diffraction data (2θ range 30─65°).

3.2.2 Deuterium desorption

The deuterium release kinetics and the corresponding phase evolutions are depicted in Fig. 5 for each desorption. The first desorption (Des1) was performed at a temperature of 270°C, starting from a deuterium pressure of 0.15 bars. However, due to the relatively high amount of sample in comparison to the experimental volume, the pressure increased progressively to reach 1.47 bars at the end of Des1. On the second (Des2) and the third (Des3) desorptions, since relatively larger amounts of deuterium were absorbed by the sample during the absorption process (Fig. 4b and Fig. 4c), the desorption pressure had to be lowered several times from about 1.5 bar to 0.15 bar to proceed with the desorption process. This was made necessary

because the driving force for the desorption reaction is strongly reduced when the hydrogen pressure tends to reach the equilibrium pressure between the metal and its hydride. Thus, deuterium was released from the sample through a discontinuous process for Des2 and Des3, as previously seen in Table 1. For Des2, the 2 first steps of deuterium desorption were carried out at T = 270 °C. Since there was still about 2.3 wt % of deuterium stored in the sample after 115 min of desorption, the desorption temperature was increased to T = 285°C for 65 minutes in order to desorb the remaining deuterium in a reasonable time, then followed by a final step under dynamic vacuum which is not reported since it was not anymore possible to record the deuterium released. For Des3, the deuterium discharging was carried out at 285 °C in 2 steps.

Table 3 gives the weight fractions of phase constituents calculated from the Rietveld refinements of neutron diffraction patterns during each desorption. For the first desorption, most of the deuterium was released from the MgD_2 phase after 90 min of discharging within one single step, as shown in Fig. 5a. However, approximately 0.68 wt % of deuterium remained in the sample in the form of MgD_2. In addition, a slight amount (about 0.23 wt %) of the $Mg_2NiD_{0.3}$ solid solution had formed upon the deuterium desorption, with a hexagonal crystal structure (P 62 2 2, a = 5.2269 Å and c = 13.3092 Å). It could be assumed that this $Mg_2NiD_{0.3}$ phase results from the desorption of the Mg_2NiD_4 phase formed during the first absorption at 250°C, even if this amount is too low to be detected at the beginning of Des1.

Fig. 5b shows the deuterium release kinetics with respect to phase evolution during the second deuterium desorption. The Mg_2NiD_4 phase formed during the Abs2 completely decomposed into $Mg_2NiD_{0.3}$ and deuterium within 6 min. Comparatively, the $MgD_2 \rightarrow Mg + D_2$ reaction proceeded rather slowly and about 2.3 wt % of deuterium was still present in the sample in the form of MgD_2 and $Mg_2NiD_{0.3}$ after 115 min. at 270°C. As the desorption temperature was increased to T = 285°C for further desorption, the sample was almost completely desorbed except for the residual deuterium present in the form of $Mg_2NiD_{0.3}$ solid solution and few

amount of MgD_2 after another 60 min. At the end of this desorption step about 3.51 wt % of $Mg_2NiD_{0.3}$ was formed, which is slightly higher than the amount of Mg_2NiD_4 present in the sample at the beginning of this desorption (2.95 wt %). This confirms that the solid solution mainly results from the decomposition of the already formed Mg_2NiD_4, although a small proportion of additional solid solution may also have formed during desorption, as suggested by the decrease in the amount of nickel. Moreover, as a further step of desorption under dynamic vacuum was applied at the end of Des2 (between 180 and 240 min., as indicated in Table 1), an additional amount of $Mg_2NiD_{0.3}$ (up to 5.14 wt %), appears simultaneously with the decrease of Ni (down to 17.56 wt %) indicating an enhance reaction under vacuum.

Table 3 Weight fractions of phase constituents calculated from Rietveld refinements of neutron diffraction patterns during deuterium desorption.

	Mg, wt %	**Ni, wt %**	**$Mg_2NiD_{0.3}$, wt %**	**MgD_2, wt %**	**Mg_2NiD_4, wt %**
Des1@270 °C					
t = 0 min	49.61 ± 0.46	24.60 ± 0.24	0.089±0.34	24.55 ± 0.19	0
t = 90 min	70.80 ± 0.55	24.65 ± 0.23	0.23±0.30	2.82 ± 0.07	0
Des2@270°C					
t = 0	22.24 ± 1.23	22.16 ± 0.47	0.25 ± 0.57	53.50 ± 0.81	2.95 ± 0.14
t = 55 min	35.20 ± 0.96	21.26 ± 0.35	2.18 ± 0.47	39.35 ± 0.48	0
t = 115 min	54.06 ± 1.03	20.81 ± 0.30	2.39 ± 0.56	20.83 ± 0.23	0
Des2@285°C t = 180 min	72.56 ± 1.18	19.91 ± 0.28	3.51 ± 0.57	2.16 ± 0.06	0
Des2@285°C **dynamic vac.** t = 240 min	73.18 ± 1.22	17.56 ± 0.26	5.14 ± 0.48	0.14 ± 0.06	0
Des3@285°C					
t =0 min	28.42 ± 1.06	15.40 ± 0.31	2.85 ± 0.55	42.64 ± 0.55	7.41 ± 0.22
t = 44 min	49.64 ± 1.41	14.96 ± 0.38	11.09 ± 0.56	23.98 ± 0.38	0
t = 104 min	69.50 ± 1.89	14.10 ± 0.40	12.69 ± 0.53	3.08 ± 0.12	0

Fig. 5c shows the deuterium release kinetics and related phase evolution during the third deuterium desorption, performed at $T = 285$ °C. As for the second desorption, the reaction proceeded in a reverse order to the deuterating process observed on the third absorption (Fig. 4d and 4e). First, the Mg_2NiD_4 transformed into the $Mg_2NiD_{0.3}$ solid solution and deuterium in a very short period of time (less than 3 minutes). Subsequently, the MgD_2 transformed into Mg and deuterium. This second stage was again a rather slow process, as confirmed in Fig. 5d by the 2D plot representing neutron diffraction patterns. After about 100 min. of desorption, there was still about 0.90 wt % of deuterium remaining in the sample in the form of $Mg_2NiD_{0.3}$ (~12.69 wt %) and MgD_2 (~3.08 wt %). The proportion of solid solution observed at the end of desorption corresponds essentially to the desorption of the Mg_2NiD_4 phase initially present at the end of absorption 3, to which is added, however, the direct formation of $Mg_2NiD_{0.3}$ as indicated by the decrease in the quantity of nickel during the reaction (from 15.4 to 14.1 wt %).

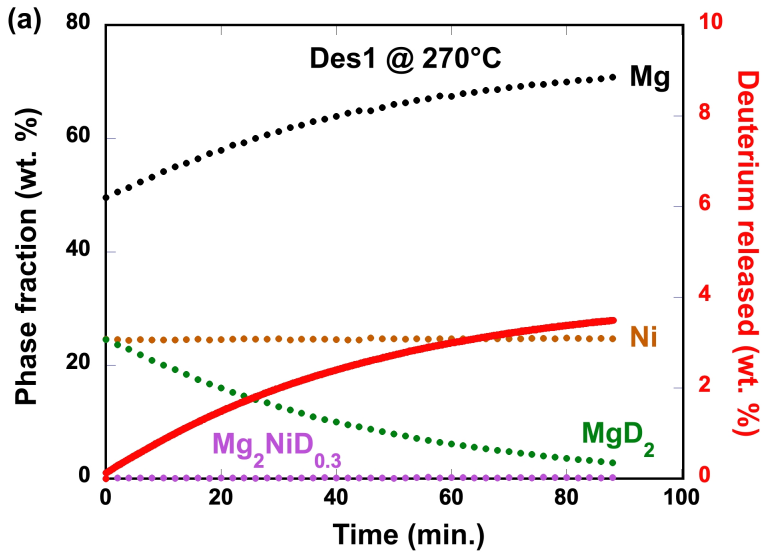

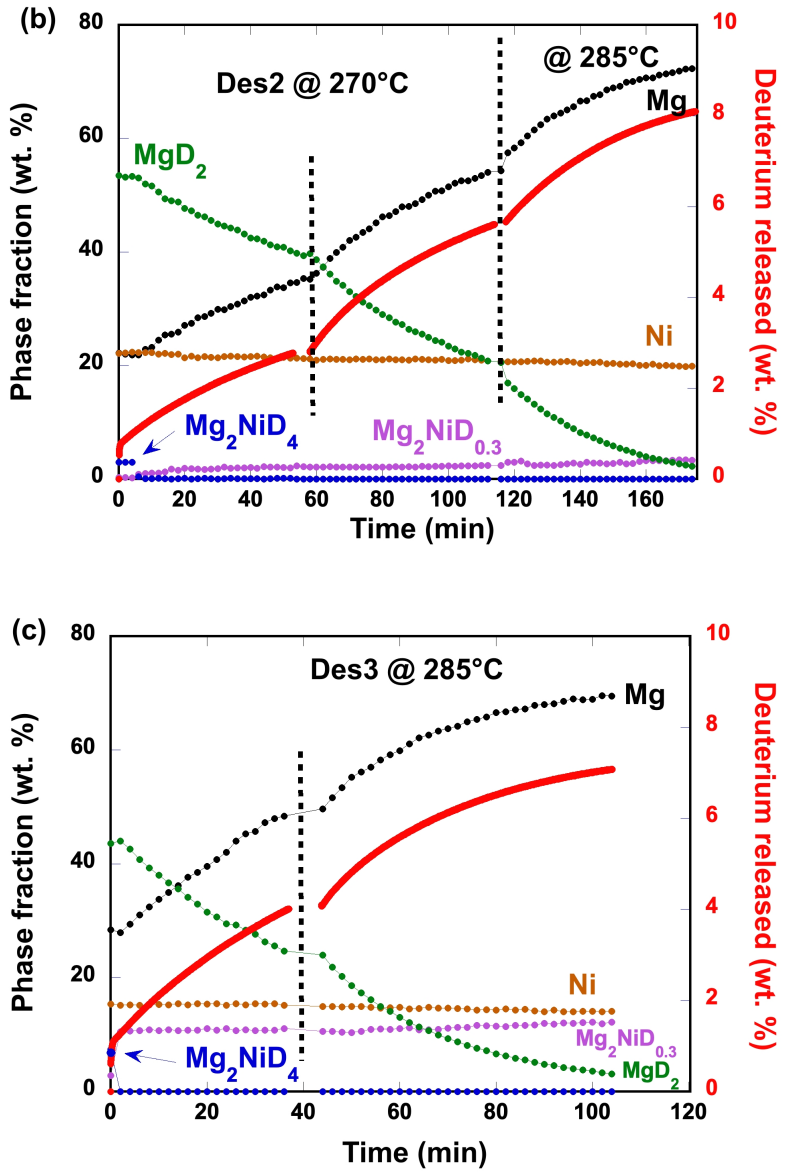

Fig. 5: Deuterium release kinetics coupled with phases evolution during each discharging process. (a) Des1 at T = 270°C and a progressive increase of the deuterium pressure from 0.15 to 1.5 bars, (b) Des2-Part1 and Part2 at T = 270 °C, Des2-Part 3 at T = 285 °C (c) Des3 at T = 285 °C. Note that the second desorption was divided into three parts and the third one into two parts, the vertical dashed lines corresponding to the deuterium pressure reductions respectively at 55 and 115 minutes for Des 2, and at 40 minutes for Des 3. (d) 2D plot of neutron diffraction patterns for Des3-Part 1.

3.3 Microstructural analysis after deuterium charging

Fig. 6 presents the microstructure of the partially deuterated sample after the 4th charging. A SEM micrograph taken from the cross section of the partially charged sample is shown in Fig.

6a. The large domains elongated along the horizontal axis are due to the flattening, on forging, of the initial larger Mg powder particles. The finer and more equiaxed domains surrounding them witness the presence of the fine and hard Ni powder particles. The progressive deuterium charging has induced internal stress and partial fragmentation of some particles. A closer analysis of the selected area shown in (Fig. 6a) is given in the following images. Fig. 6b and 6d are two SEM micrographs imaged under secondary (SEI) and back scattered (BSE) electron conditions, respectively. Fig. 6c shows the corresponding EBSD phase map, superimposed with band contrast, in which the phases Mg, Ni, MgD_2 and Mg_2NiD_4 are colored in red, yellow, green and blue, respectively. The initially compressed and elongated Mg particles are surrounded by the newly formed MgD_2 grains. A kind of sandwich-like structure MgD_2-Mg-MgD_2 was formed by MgD_2 nucleated at the periphery of the Mg powder particles and growing toward their center. A detailed analysis of the Mg grains mapped in the IPF maps in Fig. 6e and the MgD_2 domains in Fig. 6f did not reveal any preferential orientation relationship between the two phases. Although this sample is in a partially hydrided state, it was rare to encounter grains with both the deuteride (MgD_2) and the metal (Mg) phases coexisting. As indicated by the blue and yellow color in Fig. 6c, the ternary magnesium nickel deuteride Mg_2NiD_4 grains were formed at the periphery of the initial sites of the Ni powder particles. The presence of remaining Ni phase indicates that Ni was only partially alloyed with Mg through the interdiffusion of Mg and Ni upon the successive deuterium charging/discharging cycles. Approximately 45 ± 1.0 % wt % of Ni was consumed progressively to form $Mg_2NiD_{0.3}$/Mg_2NiD_4 during the different deuterium sorption cycles (Table 2 and Table 3).

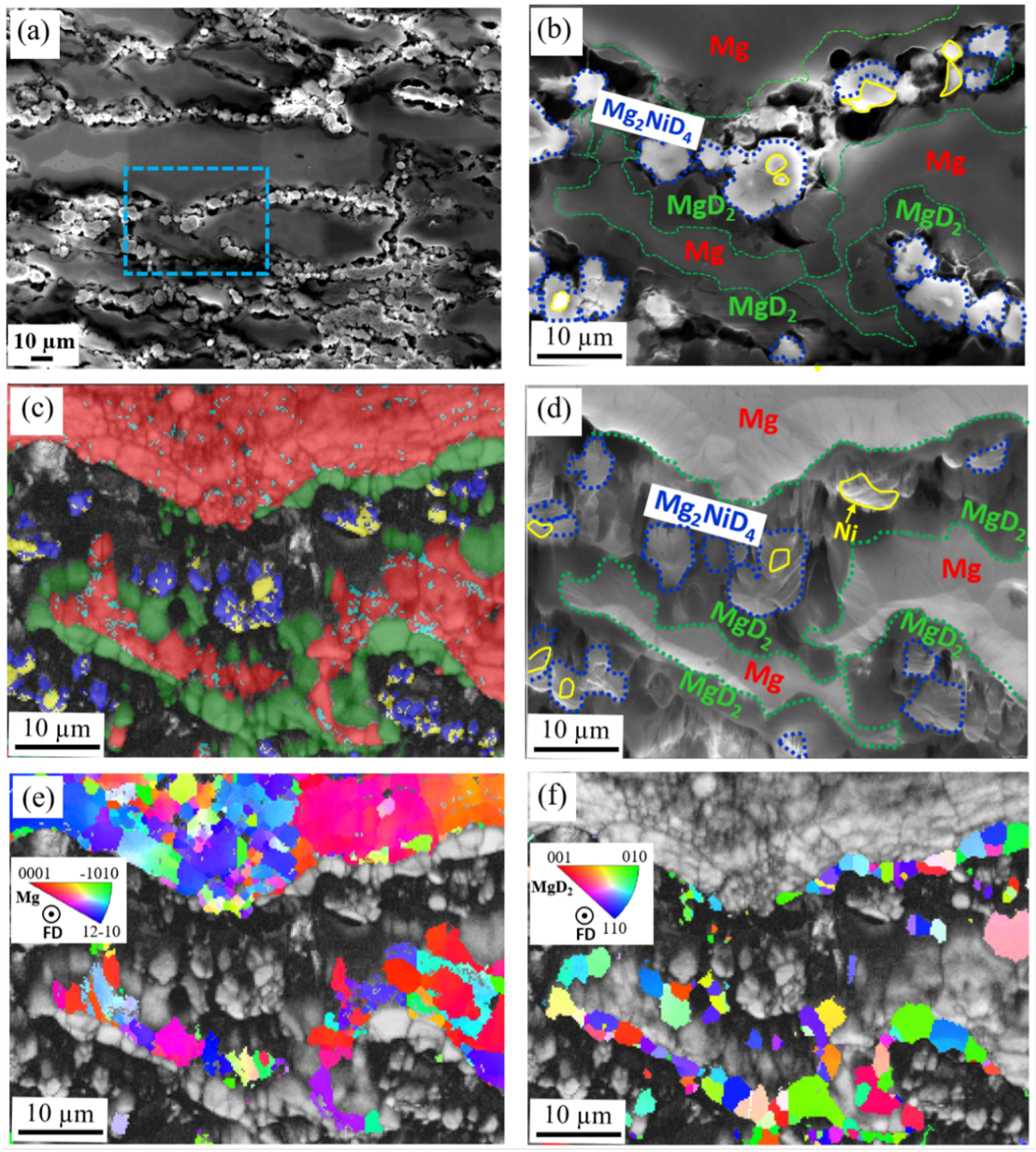

Fig. 6: Microstructure of the partially deuterated sample. (a) SEM-SEI image taken from the cross section, (b) and (d) close observation of the selected area in (a) using SEI and BSE, respectively; (c) EBSD phase map superimposed with band contrast, in which the phases Mg, Ni, MgD_2 and Mg_2NiD_4 are indicated in red, yellow, green and blue, respectively; IPF maps of Mg (e), and MgD_2 (f), respectively (the porosities are in black).

4. Discussion

This study demonstrates that deuterium absorption can occur at temperatures as low as 250 °C by forging at room temperature a compact made of a mixture of Ni and Mg powders. Although

the uptake kinetics is rather slow, this result is remarkable as the sample initially contains Ni and pure Mg particles only. There is therefore no synergistic effect as observed when the Mg_2Ni phase is present [9-10], although the hydrogenation of micro-sized Mg powders normally occurs at temperatures above at least 300 °C [35, 36]. The direct effect of cold-forging on the hydrogen uptakes has been shown in our previous work [30] for the Mg-Ni powder by comparing the behavior of the initially compacted powder mixture with the cold-forged one. The basal fiber texture as well as the structural defects induced upon cold-forging are likely to facilitate hydrogen diffusion through the sample volume leading to faster absorption rates than the one observed for the simply initially compacted powders. Indeed, Jorge Jr et al. [37] have shown that the presence of a basal fiber texture is the best orientation for hydrogen absorption while structural defects have been shown to enhance absorption kinetics [34, 35, 37-39] and lower the temperature of absorption.

The Mg_2NiD_4 forms essentially during the second absorption, performed at 270°C. Even if the formation kinetics of this phase is rather low (less than 3 wt % in a few hours), it must be recalled that it involves here the mobility of the metal atoms of Mg and/or Ni at a temperature close to about 0.5 T_m, well below the melting point of the eutectic composition (T_m = 506°C). In order to follow the global reaction of Mg and Ni, the sum of the mole fractions of the Mg_2NiD_4 phase and the solid solution $Mg_2NiD_{0.3}$ recorded at the beginning and at the end of each absorption and each desorption are plotted in Fig. 7. This figure shows that Mg and Ni are more likely to react and form Mg_2NiD_4 during the absorption process than the desorption one. The formation reaction is obviously more pronounced at 285°C, which is still a modest temperature compared to the melting temperature of the eutectic composition. The $Mg_2NiD_{0.3}$ solid solution that forms during the desorption is mostly inherited from the Mg_2NiD_4 already formed in the previous absorption stage. A slight reaction of Mg and Ni to form $Mg_2NiD_{0.3}$ is however observed when desorption takes place in low deuterium pressure regime (second part

of Des3). This recombination is even more pronounced under a dynamic vacuum regime (last step of Des2).

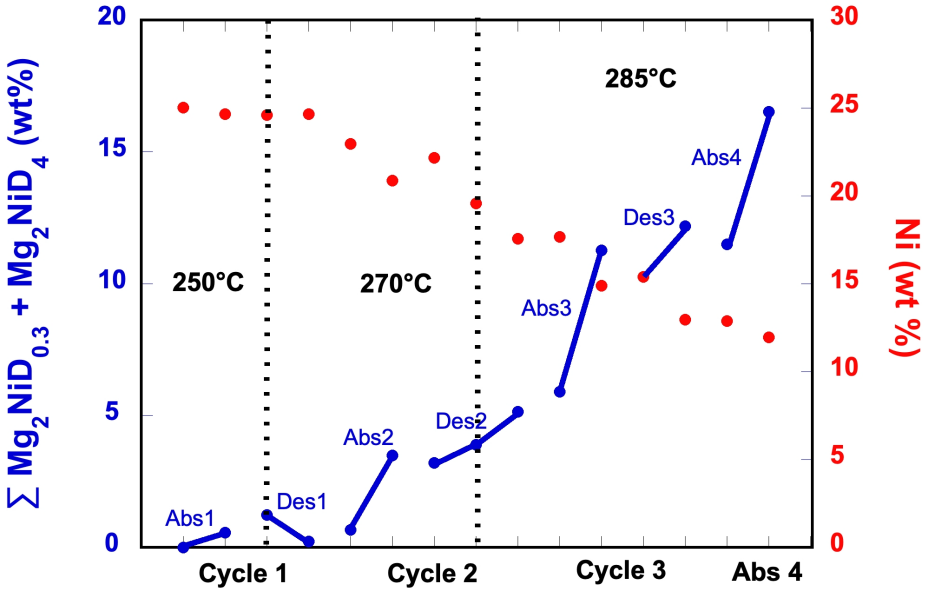

Fig. 7: Weight fraction of $Mg_2NiD_{0.3}$ + Mg_2NiD_4 at the beginning and at the end of each absorption and each desorption. Note that the 3rd point reported for Des2 corresponds to the amount achieved after desorption under dynamic vacuum.

As already mentioned, the progressive formation of Mg_2NiD_4 upon cycling is accompanied by the evolution of the absorption reaction into a multi-step process. This is most probably the result of thermodynamic considerations, the Mg_2NiD_4 hydride being less stable than MgH_2. A similar behavior was observed on samples forged in different experimental conditions, and will be discussed in a distinct paper [31]. A careful observation of Fig. 4c and Fig. 4d shows that it is mainly during stage II of the absorption, corresponding to the hydriding of the solid solution $Mg_2NiD_{0.3}$, that an additional amount of Mg_2NiD_4 appears and that the quantity of Ni decreases concomitantly. Thus, the Mg_2NiD_4 phase appears to form directly without passing through the intermediate formation of the Mg_2Ni intermetallic compound. This transformation occurs within a short period of time, during the step II of absorption. Indeed, for Abs4 (Fig. 4d) for

example, an increase of about + 6 wt % of the amount of the sum ∑ $Mg_2NiD_{0.3}$ + Mg_2NiD_4 is obtained within 12 minutes only.

The microstructure observations in Fig. 6 show that the Mg-Ni compounds are formed from the periphery of the Ni particles towards their core. This requires a fast propagation of the reaction front at the interfaces between the $Mg_2NiD_{0.3}$ or Mg_2NiD_4 phases and Ni one, using a process controlled simultaneously by the deuterium diffusion and the migration of Mg atoms through the already formed Mg_2NiD_4. For two reasons at least, such a mechanism was not obvious. Firstly, it is well established that the hydrogen diffusion in the Mg_2NiD_4 hydride is much slower than in the $Mg_2NiD_{0.3}$ solid solution [40]. Secondly, the mobility of metal atoms is expected to be rather slow at the (rather low) temperatures used here. To verify this last point, a sample forged at room temperature was heat treated for 48 hours in dynamic vacuum at 285°C. The X-ray diffraction pattern recorded after annealing revealed only Mg and Ni crystallized phases. This confirms that the temperature itself cannot explain solely any reaction between Mg and Ni even with the specific microstructure induced by cold forging. Here, the facilitated formation of Mg_2Ni-based compounds is therefore correlated to the presence of deuterium. Experimental evidence of hydrogen-induced mobility of metal atoms - under conditions in which such mobility does not occur in the absence of hydrogen - were already reported. For example, such H-lattice mobility has been observed by T. Flanagan et al., in the ordering of disordered Pd_3Mn under 50 bars of hydrogen pressure, at a temperature where ordering is too slow to be observed in the absence of hydrogen [41]. Using Pd-Rh alloys, the same group has also shown hydrogen-induced micro-segregation resulting from an enhancement of the metal atoms mobility in presence of hydrogen [42]. The mechanism of the H-induced metal mobility is not well understood. It could be of thermodynamic origin with the creation of an additional free energy contribution in the presence of hydrogen. It is also very likely that the expansion of the lattice and/or the strain accompanying the hydrogen absorption can assist the metal atoms mobility.

5. Conclusions

The aim of the present work was to determine the formation conditions of the Mg_2Ni and Mg_2NiH_4 phases at low temperature. To this end, *in situ* neutron diffraction during charging / discharging of deuterium and post-mortem EBSD observations have been carried out on a cold-forged Mg + Ni powder mixture. The main conclusions can be summarized as follows:

1) Forging compacted powders at room temperature is a simple way to develop hydrogen sorption properties in Mg-Ni compounds, making the process safe and economical for large-scale production.

2) Although the as-forged sample contains only Mg and Ni phases, the first deuterium absorption has occurred at a temperature as low as 250 °C due to the co-existence of basal fiber texture and structural defects induced by the forging process. This temperature is at least 100 °C lower than the typical temperature required for Mg and absorption could be achieved without the use of activation by ball-milling to refine the microstructure.

3) The recombination of Mg and Ni into $Mg_2NiD_{0.3}$ and/or Mg_2NiD_4 is observed from 270 °C. The Mg-Ni compounds nucleate at the periphery of the Ni particles and grow towards their core. The fast propagation of the reaction front at the interface with the Ni phase is controlled simultaneously by deuterium diffusion and migration of Mg atoms through the already formed Mg_2NiD_4. This phenomenon occurs at a particularly low temperature and is most likely promoted by an H-induced mobility of the metal atoms.

4) The MgD_2 phase initially nucleated at $Mg/Mg_2NiD_{0.3}$ interphase boundaries then grew into the center of Mg domains. This underlines the role of interphase boundaries in hydride formation. The amount of $Mg_2NiD_{0.3}$ had a drastic effect on the sequences of phase transformation as well as their kinetics:

- Without $Mg_2NiD_{0.3}$, the kinetics of absorption were controlled by the Mg → MgD_2 phase transformation resulting in a rather slow deuterium uptake.

- In the presence of $Mg_2NiD_{0.3}$, this phase catalyzed the Mg → MgD_2 phase transformation which occurred rapidly. In a second step, the kinetics of Mg → MgD_2 transformation became slower, but was compensated by the rapid $Mg_2NiD_{0.3}$→Mg_2NiD_4 transformation. Finally, after the completion of the Mg_2NiD_4 formation, the deuterium uptake occurred only via the Mg → MgD_2 transformation with a slower kinetics.

5) The deuterium desorption always proceeded in a reverse order to the deuterating process. Without Mg_2NiD_4, the deuterium desorption was controlled by the MgD_2 → Mg + D_2 reaction and lasted for a long time, whereas in the presence of Mg_2NiD_4, the release of deuterium started by its rapid decomposition followed by a slower MgD_2 decomposition process.

Acknowledgement

This work was supported by the IDEX-CDP Eco-SESA program from the Université Grenoble Alpes and the French State through the program "Investment in the future" operated by the National Research Agency (ANR) and referenced by ANR-11-LABX-0008-01 (Labex DAMAS). 2FDN (Fédération Française de Diffusion Neutronique) is acknowledged for beam time allocation and the skillful assistance from the CRG-D1b team and Simon Beaudouin from the Institute Laue Langevin (ILL) neutron source in Grenoble (France) were greatly appreciated. Dr. WEN Jing thanks the National Natural Science Foundation of China (No. 52201241) for financial support.

References

[1] A. Zaluska, L. Zaluski, J.O. Ström-Olsen, Nanocrystalline magnesium for hydrogen storage, J. Alloys Compd. 288 (1999) 217-225. https://doi.org/10.1016/S0925-8388(99)00073-0

[2] B. Sakintuna, F. Lamari-Darkrim, M. Hirscher, Metal hydride materials for solid hydrogen storage: a review, Int. J. Hydrogen Energy 32 (2007) 1121-1140. https://doi.org/10.1016/j.ijhydene.2006.11.022

[3] I.P. Jain, C. Lal, A. Jain, Hydrogen storage in Mg: a most promising material, Int. J. Hydrogen Energy 35 (2010) 5133-5144. https://doi.org/10.1016/j.ijhydene.2009.08.088

[4] V.A. Yartys, M.V. Lototskyy, E. Akiba, R. Albert, V.E. Antonov, J.R. Ares, M. Baricco, N. Bourgeois, C.E. Buckley, J.M. Bellosta von Colbe, J.C. Crivello, F. Cuevas, R.V. Denys, M. Dornheim, M. Felderhoff, D.M. Grant, B.C. Hauback, T.D. Humphries, I. Jacob, T.R. Jensen, P.E. de Jong, J.M. Joubert, M.A. Kuzovnikov, M. Latroche, M. Paskevicius, L. Pasquini, L. Popilevsky, V. M. Skripnyuk, E. Rabkin, M.V. Sofianos, A. Stuart, G. Walker, Hui Wang, C.J. Webb, Min Zhu, Magnesium based materials for hydrogen based energy storage: Past, present and future, Int. J. Hydrogen Energy 44 (2019) 7809-7859. https://doi-org.inp.bib.cnrs.fr/10.1016/j.ijhydene.2018.12.212

[5] J. Huot, G. Liang, S. Boily, A. van Neste, R. Schultz, Structural study and hydrogen sorption kinetics of ball-milled magnesium hydride, J. Alloys Compd. 293-295 (1999) 495-500. https://doi.org/10.1016/S0925-8388(99)00474-0

[6] J.L. Bobet, B. Chevalier, M.Y. Song, B. Darriet, J. Etourneau, Hydrogen sorption of Mg-based mixtures elaborated by reactive mechanical grinding, J. Alloys Compd. 336 (2002) 292-296. https://doi.org/10.1016/S0925-8388(01)01883-7

[7] G. Barkhordarian, T. Klassen, R. Bormann, Effect of Nb_2O_5 content on hydrogen reaction kinetics of Mg, J. Alloys Compd. 364 (2004) 242-246. https://doi.org/10.1016/S0925-8388(03)00530-9

[8] H. Simchi, A. Kaflou, A. Simchi, Synergetic effect of Ni and Nb_2O_5 on dehydrogenation properties of nanostructured MgH_2 synthesized by high-energy mechanical alloying, Int. J. Hydrogen Energy 34(2009)7724-7730. https://doi.org/10.1016/j.ijhydene.2009.07.038

[9] J.J. Reilly Jr, R.H. Wiswall Jr, The Reaction of hydrogen with alloys of magnesium and nickel and the formation of Mg_2NiH_4, Inorg. Chem. 7 (1968) 2254-2256.

[10] A. Zaluska, L. Zaluski, J.O. Strom-Olsen, Synergy of hydrogen sorption in ball-milled hydrides of Mg and Mg_2Ni, J. Alloys. Compd. 289 (1999) 197-206. https://doi.org/10.1016/S0166-0462(99)00013-7

[11] S. Kalinichenka, L. Röntzschb, B. Kieback, Structural and hydrogen storage properties of melt-spun Mg-Ni-Y alloys, Int. J. Hydrogen Energy 34 (2009) 7749-7755. https://doi.org/10.1016/j.ijhydene.2009.07.053

[12] X.J. Hou, R. Hu, T.B. Zhang, H.C. Kou, J.S. Li, Hydrogenation thermodynamics of melt-spun magnesium rich Mg-Ni nanocrystalline alloys with the addition of multiwalled carbon nanotubes and TiF_3, J. Power Sources 306 (2016) 437-447. https://doi.org/10.1016/j.jpowsour.2015.12.050

[13] K. Edalati, A. Bachmaier, V. A. Beloshenko, Y. Beygelzimer, V.D. Blank and W.J. Botta, Nanomaterials by server plastic deformation: review of historical developments and recent

advances, Materials research Letters 10 (4), 2022. https://doi.org/10.1080/21663831.2022.2029779

[14] W.J. Botta, G. Zepon, T.T. Ishikawa, D.R. Leiva, Metallurgical processing of Mg and MgH_2 for hydrogen storage, J. Alloys Compd. 897 (2022) 162798. https://doi.org/10.1016/j.jallcom.2021.162798

[15] K. Edalati, E. Akiba, W. J. Botta, Y. Estrin, R. Floriano, D. Fruchart, T. Grosdidier, Z.J. Horita, J. Huot, H.W. Li, H.J. Lin, Á. Révész and M. J. Zehetbauer, Impact of Severe Plastic Deformation on Kinetics and Thermodynamics of Hydrogen Storage in Magnesium and Its Alloys, J. Mater. Sci. Technol. 146, (2023), 221-239. https://doi.org/10.1016/j.jmst.2022.10.068

[16] V. Skripnyuk, E. Buchmann, E. Rabkin, Y. Estrin, M/ Popov, S. Jorgensen, The effect of equal angular pressing on hydrogen storage properties of a eutectic Mg-Ni alloy, J. Alloys Compd. 436 (2007) 99-106. http://dx.doi.org/10.1016/j.jallcom.2006.07.030

[17] L. Popilevsky, V.M. Skripnyuk, Y. Estrin, A. Dahle, D. Mirabile Gattia, A. Montone, E. Rabkin, Hydrogenation-induced microstructure evolution in as cast and severely deformed Mg-10 wt.% Ni alloy, Int. J. Hydrogen Energy 38 (2013) 12103-12114. https://doi.org/10.1016/j.ijhydene.2013.03.034

[18] S.J. Huang, V. Rajagopal, A. N. Ali, Influence of the ECAP and HEBM processes and the addition of Ni catalyst on the hydrogen storage properties of AZ31-x Ni (x=0,2,4) alloy, Int. J. Hydrogen Energy 44 (2019) 1047-1058. https://doi.org/10.1016/j.ijhydene.2018.11.005

[19] A. Revesz, Zs. Kanya, T. Verebelyi, P.J. Szabo, A.P. Zhilyaev, T. Spassov, The effect of high-pressure torsion on the microstructure and hydrogen absorption kinetics of ball-milled $Mg_{70}Ni_{30}$, J. Alloys Compd. 504 (2010) 83-88. https://doi.org/10.1016/j.jallcom.2010.05.058

[20] T. Grosdidier, J.J. Funderberger, J.X. Zou, Y.C. Pan, X.Q. Zeng, Nanostructured Mg based hydrogen storage bulk materials prepared by high pressure torsion consolidation of arc plasma evaporates ultrafine powders, Int. J. Hydrogen Energy 40 (2015) 1685-1691. https://doi.org/10.1016/j.ijhydene.2015.06.159

[21] M. Gajdics, M. Calizzi, L. Pasquini, E. Schafler, Characterization of a nanocrystalline Mg Ni alloy processed by high-pressure torsion during hydrogenation and dehydrogenation, Int. J. Hydrogen Energy 41 (2016) 9803-9809. https://doi.org/10.1016/j.ijhydene.2015.12.224

[22] M. Osorio-Garcia, K. Suarez-Alcantara, Y. Todaka, A. Tejeda-ochoa, M. Herreara-ramirez, O. Hernandez-Silva, F. Cruz-Gandarilla, J.G. Cabanas-Moreno, Low-temperature hydrogenation of Mg-Ni-Nb_2O_5 alloy processed by high-pressure-torsion, J. Alloys Compd. 878 (2021) 160309. https://doi.org/10.1016/j.jallcom.2021.160309

[23] T. Hongo, K. Eladati, M. Arita, J. Matsuda, E. Akiba and Z. Horita, Significance of grain boundaries and stacking faults on hydrogen storage properties of Mg_2Ni intermetallics processed by high-pressure torsion, Acta Materialia 92 (2015) 46-54. https://doi.org/10.1016/j.actamat.2015.03.036

[24] A. Revesz, M. Gajdics, E. Schafler, M. Calizzi, L. Pasquini, Dehydrogenation hydrogenation characteristics of nanocrystalline Mg_2Ni powders compacted by high-pressure torsion, J. Alloys Compd. 702 (2017) 84-91. https://doi.org/10.1016/j.jallcom.2017.01.261

[25] D.R. Leiva, H.C. de Almeida Costa, J. Huot, Magnesium nickel alloy for hydrogen storage produced by malt spinning followed by cold rolling, Materials Research 2012; 15(5), 813-817. https://doi.org/10.1590/S1516-14392012005000096

[26] A. Revesz, M. Gajdics, L.K. Varga, G. Krallics, L. Peter, T. Spassov, Hydrogen storage of nanocrystalline Mg-Ni alloy processed by equal-channel angular pressing and cold rolling, Int. J. Hydrogen Energy 39 (2014) 9911-9917. http://dx.doi.org/10.1016/j.ijhydene.2014.01.059

[27] A.A. Cesario Asselli, D.R. Leiva, G.H. Cozentino, R. Floriano, J. Hupt, T.T. Ishikawa, W. J. Botta, Hydrogen storage properties of MgH_2 processed by cold forging, J. Alloys Compd. 615 (2014) S719-S724. https://doi.org/10.1016/j.jallcom.2014.01.065

[28] J. Huot, S. Amira, J. Lang, N. Skryabia, D. Fruchart, Improvement of hydrogen properties of magnesium alloys by cold rolling and forging, Mater. Sci. Eng. 63 (2014) 012-114. https://doi.org/10.1088/1757-899X/63/1/012114

[29] P. de Rango, J. Wen, N. Skryabina, Hydrogen storage properties of Mg-Ni alloys proceed by fast forging, Energies MDPI, 2020, 13 (13), pp.3509. https://doi.org/10.3390/en13133509

[30] J. Wen, P. de Rango, N. Allain, L. Laversenne, T. Grosdidier, Improving hydrogen storage performance of Mg-based alloy through microstructure optimization, J. Power Sources 480 (2020) 228823. https://doi.org/10.1016/j.jpowsour.2020.228823

[31] J. Wen, P. de Rango, M. Novelli, T. Grosdidier and L. Laversenne, In-situ investigation of hydrogen sorption mechanisms in forged Mg-Mg_2Ni composites, using neutron diffraction, to be submitted.

[32] I. Popa, P. de Rango, D. Fruchart, S. Rivoirard, High-speed forged NdFe12-XVX compounds for bonded magnets, J. Mag. Mater. 242-245 (2002) 1388-1390.

[33] J. Rodriguez-Carvajal, Recent developments of the program FULLPROF, Commission Powder Diffraction Newslett, 26 (2001) 12-19.

[34] Y.N. Wang, J.C. Huang, Texture analysis in hexagonal materials, Mater. Chem. Phys. 81 (2003) 11-26. https://doi.org/10.1016/S0254-0584(03)00168-8

[35] C.P. Chen, B.H. Liu, Z.P. Li, J. Wu, Q.D. Wang, The activation mechanism of Mg-based hydrogen storage alloys, Phys. Chem. 181 (1993) 259-267. https://doi.org/10.1016/S0360-3199(98)00039-1

[36] S. Panda, J.J. Fundenberger, Y. Zhao, J. Zou, L.S. Toth, T. Grosdidier, Effect of initial powder type on the hydrogen storage properties of high-pressure torsion consolidated Mg, Int. J. Hydrog. Energy 42 (2017) 22438-22448. https://doi.org/10.1016/j.ijhydene.2017.05.097

[37] A.M. Jorge Jr., G.F. de Lima, M.R. Martins Triques, W.J. Botta, C.S. Kiminami, R.P. Nogueira, A.R. Yavari, T.G. Langdon, Correlation between hydrogen storage properties and textures induced in magnesium through ECAP and cold rolling, Int. J. Hydrogen Energy 39 (2014) 3810-3821. https://doi.org/10.1016/j.ijhydene.2013.12.154

[38] K. Edalati, A. Yamamoto, Z. Horita, T. Ishihara, High-pressure torsion of pure magnesium: Evolution of mechanical properties, microstructures and hydrogen storage capacity with equivalent strain, Scr. Mater. 64 (2011) 880-883. https://doi.org/10.1016/j.scriptamat.2011.01.023

[39] T. Grosdidier, J.J. Fundenberger, J.X. Zou, Y.C. Pan, X.Q. Zeng, Nanostructured Mg based hydrogen storage bulk materials prepared by high pressure torsion consolidation of arc plasma evaporated ultrafine powders, Int. J. Hydrogen Energy 40 (2015) 16985-16991. https://doi.org/10.1016/j.ijhydene.2015.06.159

[40] J. Cermak, L. Kral, Hydrogen diffusion in Mg-H and Mg-Ni-H alloys, Acta Mater. 56 (2008) 2677-2686. https://doi.org/10.1016/j.actamat.2008.02.003

[41] T. Flanagan, A.P. Craft, T. Kuji, K. Baba and Y. Sakamoto, Hydrogen induced disordered-ordered transition in Pd_3Mn, Scr. Mater., 20 (1986) 1745-1750.

[42] H. Noh, T. Flanagan, B. Cerundolo, A. Craft, Hydrogen-induced metal atom mobility in palladium-rhodium alloys, Scr. Mater., 25 (1991)225-230.